A model for the injection boundary conditions in the context of 3D Simulation of Diesel Spray: Methodology and Validation

Lionel Martinez [a,*] Adlène Benkenida [a], Bénédicte Cuenot [b]

[a] *IFP, 1 et 4 avenue Bois Préau, 92852, Rueil Malmaison Cedex, France*

[b] *CERFACS, 4 avenue G. Coriolis , 31055, Toulouse Cedex 01, France*

Abstract

Downstream Inflow Turbulent Boundary Conditions (DITurBC) are presented for the Eulerian-Eulerian Large Eddy Simulation (LES) or Reynolds Average Navier-Stokes (RANS) Simulation of Diesel sprays. These boundary conditions initiate the spray physics close to the nozzle exit, which avoids the difficulties linked to the 3D simulation of cavitation, primary break-up and turbulence in the near-nozzle region. An injector model is combined with mass and axial momentum conservation equations to obtain mean profiles of velocity, volume fraction and droplet diameter at a given distance downstream from the nozzle exit. In order to take into account the unsteadiness of the flow, velocity fluctuations are added to the mean profile. These boundary conditions are assessed by comparison with data on injection velocity, spray angle and velocity profiles from numerous experiments.

Key words:

Boundary condition, spray, Large Eddy Simulation (LES), modelling, Diesel injection

1 Introduction

Car manufacturers are facing increasingly severe regulations on pollutant emissions and fuel consumption. To respect these regulations, new combustion concepts in Internal Combustion (IC) Engines are being developed. The HCCI (Homogeneous Charge Compression Ignition) combustion [1, 2] represents one of these concepts. Although it has shown a great potential, it still requires a comprehensive work to allow a better understanding, especially with respect to cyclic variabilities which can appear in some operating conditions. These variabilities can have a strong effect on fuel consumption and pollutants as shown by Ozdor et al [3]. The non-deterministic character of the turbulence is one of the phenomena leading to the cyclic variability. It corresponds to the microscopic events that can influence the instantaneous velocity field and the local mixture leading to different heat release, pollutant levels and engine work from cycle to cycle.

Computational Fluid Dynamics (CFD) is a helpful tool for studying such issues. The RANS (Reynolds Averaged Navier-Stokes) approach [4] is commonly used in CFD to perform 3D simulations [5]. However, although it is characterised by reasonable computational costs, it does not allow the study of the origins of cyclic variabilities: RANS calculation of a given engine operation point represents the statistical average of many cycles at this point.

Large Eddy Simulation (LES) seems to be better adapted for such studies, as one LES of a given engine operation point corresponds to one individual engine cycle, computing local and instantaneous filtered properties [6]. LES

* Corresponding author. Tel.: 33-1-47-52-6000; fax: 33-1-47-52-7068
Email address: lionel.martinez@ifp.fr (Lionel Martinez).

has demonstrated its capabilities in many configurations [7, 8] and in particular in multi-cycle simulation of IC engine [9, 10]. Moreover, due to its potential to resolve large scale vortices and so to predict the interaction between drops and air (carrier phase), LES is also of great interest for spray simulations. Indeed, knowing the level of turbulence intensity generated by the spray as well as the composition of the gas mixture is of great importance for understanding and modelling combustion in IC engines.

In this work, an Eulerian method is used for the liquid phase and preferred to the Lagrangian approaches which are commonly used in CFD. Among all limitations [11, 12, 13], one of the main drawback of Lagrangian methods is that a high particle number density is needed to achieve a satisfactory accuracy for LES. This leads to a high computational cost that is not relevant in industrial applications. This may be overcome by parallelisation but this is still delicate today, mainly due to load imbalance when particles concentrate in some processors.

The main difficulty in the simulation of a Diesel spray is the complexity of the physics at the nozzle exit for both the liquid and gas phases.This complexity leads to important difficulties for the modeling and the experimental validation.

For example, the physics at the nozzle exit is strongly linked to the behavior of the liquid flow inside the injector. Cavitation may occur, depending on the injector geometry [14] and the flow, and has strong influence on the spray velocity, angle and atomisation [15, 16, 17]. Furthermore, due to the high speed and high density of the liquid jet, traditional optical methods show limitations for the measurements in the dense liquid spray region. Therefore

the primary break-up is difficult to observe experimentally and corresponding models are not easy to validate. In addition, numerical issues arise linked to the high liquid volume fraction and the high velocities (between $400m.s^{-1}$ and $600m.s^{-1}$) emphasised by the very small scales of the physics at the nozzle exit. For instance, typical Diesel injectors have diameters (D_{exit}) between $100\mu m$ and $200\mu m$. Consequently, when using LES solvers to compute the turbulent mixing layer at the nozzle exit, one has to increase the spatial resolution. The resulting simulation cost is then prohibitive for industrial applications.

As a result of these difficulties, a methodology is proposed for injection boundary conditions to initiate the spray physics at a given distance, downstream from the nozzle exit. This new Downstream Inflow Turbulent Boundary Conditions (DITurBC) model is presented in the following sections. It has been developed in the context of LES but could be used for RANS simulations.

The paper is organised as follows Section 2 explains the methodology developed for the initialization of Diesel sprays in IC engines. The injector model is presented in Section 3 and the resulting profiles from the DITurBC model are depicted in Section 4. The model validation is described in the last Section.

2 Methodology for the initialisation of sprays in IC engines

2.1 Methodology

In order to initiate the spray physics downstream from the nozzle exit, an injector model is first used to estimate the properties of the flow at the nozzle exit such as the liquid velocity, the effective exit section and the spray angle.

Then based on these results and using conservation equations, the velocities of gas and liquid, the volume fraction and the droplet size profiles are deduced on a 2D plane located at a distance *Dist* downstream from the nozzle exit, called the DITurBC plane (see Fig. 1). These profiles represent the Downstream Inflow Turbulent Boundary Conditions (DITurBC) that will be used to initiate Eulerian-Eulerian LES of spray injection.

2.2 Distance to nozzle exit

A review of experimental results concerning the spray structure and break up mechanisms has been conducted by Smallwood et al. [18] for Diesel injection.

The first observation is that the spray is completely atomised very closed to the nozzle tip. This analysis is confirmed by Ueki et al. [19] who concluded that the jet disintegration was complete at $7.5D_{exit}$. This means that downstream of this distance, there is no more primary break-up and the jet is fully dispersed. Secondary break-up is nevertheless still present. This early disintegration is mainly due to turbulence effects, cavitation and secondary flow inside the injector nozzle [20]. It is important as it contributes to the spray opening. Furthermore, at this distance, liquid velocity, volume fraction or droplet size mean profiles are Gaussian [21, 22, 19].

Based on this studies, it is proposed to apply boundary conditions at a distance of 10 nozzle diameters from the injector tip. At this distance and considering the typical near spray angles of Diesel injectors ($5 - 15$ degrees), the spray width is between $0.8mm$ and $1.6mm$. With about ten nodes of the computational grid at the inlet, this lead to a minimum edge length between $80\mu m$

and $160\mu m$ which represents a good compromise between accuracy and computational cost for a LES of spray in IC engines.

3 Injector model for Diesel like injection

3.1 Principle

Knowing geometrical data of the nozzle, injection conditions and conditions in the combustion chamber, a model is built to predict first the spray velocity at the nozzle exit as well as the spray angle. Then the velocity, volume fraction and droplet size mean profiles are constructed at $Dist = 10D_{exit}$ on the DITurBC plane (see Section 4).

3.2 Determination of the velocity at the nozzle exit and the effective section area

The velocity of the liquid jet at the nozzle exit, U_{exit}, depends on whether the flow inside the injector is cavitating or merely turbulent. To determine the flow regime, the model of Sarre et al. [23] is used.

It is assumed that only two types of flow regimes can occur inside the nozzle (see Fig. 2):

- If the pressure in the *vena contracta*, P_{vena}, is larger than the saturation vapor pressure, P_{vap}, then the flow is merely turbulent ;
- Otherwise, the flow is turbulent and cavitating.

The decrease of pressure in the *vena contracta* is due to the contraction of streamlines that creates a negative pressure gradient. The pressure decreases in some areas and locally falls below the saturation vapor pressure. In this case cavitating bubbles appear inside the nozzle and contribute to the unsteadiness of the flow. Cavitation leads to a decrease of the effective area at the nozzle exit.

The conditions of transition to a cavitating flow are strongly linked to the geometrical parameters of the nozzle such as the curvature radius R, the nozzle length L, the geometrical diameter of the nozzle hole D_{exit} (see Fig. 2).

In the case of a cavitating flow the Bernoulli's equation between the region upstream from the nozzle and the *vena contracta* gives:

$$P_{vena} = P_{inj} - \frac{\rho_l}{2} U_{vena}^2 \tag{1}$$

where P_{inj} is the injection pressure, ρ_l the liquid density and U_{vena} the velocity at the smallest flow area. Following the expression of Nurick [24] for the contraction coefficient C_c and assuming a flat velocity profile, one obtains $U_{vena} = \frac{Umean}{Cc}$ and $C_c = \left(\left(\frac{\Pi+2}{\Pi} \right)^2 - 11.4R/D_{exit} \right)$ where U_{mean} is the mean velocity corresponding to the mean mass flow rate at the nozzle exit.

Then:

$$P_{vena} = P_{inj} - \frac{\rho_l}{2} \frac{U_{mean}^2}{C_c^2} \tag{2}$$

Because of the discharge loss involving a discharge coefficient C_d , the mean velocity at the nozzle exit is not the velocity predicted by Bernoulli's equation :

$$U_{mean} = C_d \underbrace{\sqrt{\frac{2\left(P_{inj} - P_{ch}\right)}{\rho_l}}}_{\text{Bernoulli's velocity}} \tag{3}$$

where

$$C_d = \frac{1}{\sqrt{K_{inlet} + f.\frac{L}{D_{exit}} + 1}} \tag{4}$$

in the case of a turbulent flow. K_{inlet} is the inlet loss coefficient and f the Blasius' coefficient for the laminar equation for wall friction: $f = max(0.316R_e^{-0.25}, 64/R_e)$ and K_{inlet} is tabulated according to Benedict [25].

Then:

$$P_{vena} = P_{inj} - \frac{C_d^2}{C_c^2}\left(P_{inj} - P_{ch}\right) \tag{5}$$

If $P_{vena} > P_{vap}$, there is no transition to cavitating flow. In this case the effective area is the geometrical area of the nozzle hole ($D_{eff} = D_{exit}$)

The exit velocity U_{exit} is then:

$$U_{exit} = U_{mean} = C_d\sqrt{\frac{2\left(P_{inj} - P_{ch}\right)}{\rho_l}} \tag{6}$$

If $P_{vena} < P_{vap}$, the flow is fully cavitating and cavitation bubbles escape from the nozzle exit. In this case, the effective section area is not the geometrical area of the nozzle hole ($D_{eff} < D_{exit}$). A new discharge coefficient is calculated as:

$$C_d = C_c\sqrt{\frac{P_{inj} - P_{vap}}{P_{inj} - P_{ch}}} \tag{7}$$

The velocity in the *vena contracta* becomes:

$$U_{vena} = \sqrt{\frac{2\,(P_{inj} - P_{vap})}{\rho_l}} \tag{8}$$

Finally, U_{exit} and the effective exit section A_{eff} are obtained by application of the conservation equations of mass and momentum between the *vena contracta* and the nozzle exit:

$$U_{exit} = U_{vena} - \frac{(P_{ch} - P_{vap})}{\rho_l . U_{mean}} \tag{9}$$

$$A_{eff} = A_{exit} \frac{U_{mean}}{U_{exit}} \tag{10}$$

with $A_{exit} = \pi D_{exit}^2 / 4$

Once the exit velocity and the effective exit section have been determined, it is necessary to calculate the spray angle. This is done below.

3.3 Spray angle at nozzle exit

The determination of the spray angle is done by assuming that the spray angle at the nozzle exit is due to the atomisation produced by the turbulence and the cavitation inside the nozzle. The atomisation model used in this work is inspired by the primary break-up model of Nishimura et al. [26]. The liquid jet atomisation produces droplets with a radial velocity that is due to the turbulent and cavitation energies which have to be determined. Then, the combination of the axial and radial components of these velocities gives the spray angle.

3.3.1 Turbulent kinetic energy due to high velocities

The turbulent kinetic energy k_{flow} of the flow inside the nozzle is given by the following empirical formula from Huh et al. [27]:

$$k_{flow} = \frac{U_{exit}^2}{8L/D_{exit}} \left(\frac{1}{C_d^2} - K_{inlet} - 1 \right) \tag{11}$$

This energy is generated by the high velocities inside the nozzle and the formula is obtained using simple overall mass, momentum, and energy balances. It is only valid for quasi-steady injection conditions.

3.3.2 Cavitation energy

Cavitation energy is defined as the energy created by the collapse of bubbles or cavitation pockets inside the nozzle. This provides an increase of turbulent energy of the liquid.

When a cavitation pocket of volume V_p collapses, the energy E_{cav} given to the surrounding flow at static pressure P is then:

$$E_{cav} \approx \int_0^{V_p} P dV \tag{12}$$

Assuming that the liquid pressure in the nozzle is homogeneous and close to the pressure in the chamber, one gets:

$$E_{cav} \approx \int_0^{V_p} P dV = \int_0^{V_p} P_{ch} dV = V_p P_{ch} \tag{13}$$

For a liquid column or ligament of total mass m_t, mass density $\rho_t \approx \rho_l$ and total

volume V_t with n_p pockets, the kinetic energy k_{cav} provided by the cavitation is:

$$k_{cav} = \frac{1}{m_t} \sum_{k=0}^{n_p} V_{p_k} P_{ch} = \frac{P_{ch}}{m_t} \sum_{k=0}^{n_p} V_{p_k} = \frac{P_{ch}}{\rho_l} \frac{\sum_{k=0}^{n_p} V_{p_k}}{V_t} = \frac{P_{ch}}{\rho_l} \frac{V_g}{V_t} \tag{14}$$

The gas volume fraction, V_g/V_t, can be determined from the effective section area previously calculated, assuming:

$$\frac{V_g}{V_t} \approx \frac{\text{Cavitation area}}{\text{Total area}} = \frac{A_{exit} - A_{eff}}{A_{exit}} \tag{15}$$

Using Eq. (15) in Eq. (14), one obtains:

$$k_{cav} = \frac{P_{ch}}{\rho_l} \left(\frac{A_{exit} - A_{eff}}{A_{exit}} \right) \tag{16}$$

The main advantage of this method is that it does not require the calculation of the pocket or bubble size, nor the bubble number, which are difficult to evaluate.

3.3.3 Determination of the spray angle at nozzle exit

The total fluctuating kinetic energy k_{tot} is the sum of the turbulent kinetic energy k_{flow} and the energy provided by the cavitation k_{cav}:

$$k_{tot} = k_{flow} + k_{cav} \tag{17}$$

This fluctuating kinetic energy provides a fluctuating velocity u', assumed to be equal to the radial velocity U_{rad} of the liquid flow at the nozzle exit . The turbulence is considered isotropic so that:

$$U_{rad} = u' = \sqrt{\frac{2}{3} k_{tot}} \tag{18}$$

The spray angle ϕ_{exit} at the nozzle exit (see Fig. 3) is then:

$$\tan\left(\phi_{exit}/2\right) = \frac{U_{rad}}{U_{exit}} \tag{19}$$

The injector model presented here permits to obtain the effective section (Eq. (10)), the velocity (Eq. (6) and Eq. (9)), and the spray angle (Eq. (19)) at the nozzle exit.

4 Modelling for the DITurBC

From the spray characteristics at the nozzle exit, determined in the previous section, the mean profiles imposed downstream on the injection plane (DITurBC) are now computed. For this purpose, mass and momentum conservation equations have to be used. A velocity fluctuation is then added to the mean profile in order to take into account the unsteadiness of the flow.

4.1 Spray angle at $10D_{exit}$ from nozzle exit

The angle ϕ_{exit} calculated by the injector model differs from the spray angle ϕ_{aero} far from the nozzle exit (see Fig 3). Indeed, ϕ_{exit} is mainly due to the injection condition and the shape of the nozzle whereas ϕ_{aero} is controlled by aerodynamics (gas density and turbulence) and depends on conditions in the chamber [23]. To estimate if aerodynamic effects have sufficient time to affect the spray angle of the DIturBC, the characteristic aerodynamic time τ_{aero} is

compared to the convective time $\tau_{conv} = Dist/U_{exit}$:

Following [23], the aerodynamic spray angle, based on empirical considerations, is:

$$\tan(\phi_{aero}/2) = \frac{4\pi}{A}\sqrt{\frac{\rho_g}{\rho_l}} f(T) \tag{20}$$

where A and T are parameters set to $A = 4.4$ and $T = \left(\frac{Re}{We}\right)^2 \frac{\rho_g}{\rho_l}$ and $f(T) = \left(\sqrt{3}/6\,(1 - \exp(-10T))\right)$ and We is the weber number. According to [23], this equation predicts spray angles very close to measured values.

The aerodynamic time is linked to the density ratio and evaluated with the nozzle diameter and the exit velocity:

$$\tau_{aero} = C\sqrt{\frac{\rho_l}{\rho_g}}\frac{D_{exit}/2}{U_{exit}} \tag{21}$$

C is an additional constant empirically fixed by [28] at the value $C = 1.73$.

If $\tau_{conv} < \tau_{aero}$, aerodynamic effects are negligible and the spray angle ϕ of the DITurBC is $\phi = \phi_{exit}$.

If $\tau_{conv} \geq \tau_{aero}$, ϕ is calculated with a simple geometrical law (see Fig. 3):

$$\tan(\phi/2) = \frac{\tau_{aero}}{\tau_{conv}}\tan(\phi_{exit}/2) + \left(1 - \frac{\tau_{aero}}{\tau_{conv}}\right)\tan(\phi_{aero}/2) \tag{22}$$

4.2 Radial Distributions Profiles

In this section, the radial profiles of liquid volume fraction α_l, axial velocity U_{axial}, radial velocity U_{rad} and droplet size d are determined. Experimental measurements from [21] using X-ray absorption in the near-nozzle region have

shown that radial distributions of liquid volume fraction are well described by a Gaussian distribution. Furthermore, according to Chaves et al. [29] , radial distributions of mean axial velocity are near Gaussian. Lastly, according to Ueki et al. [19], who measured droplet sizes and velocities near the injector exit, the radial distributions of axial velocity and droplet diameter are correlated and Gaussian. Based on these experiments, the radial distribution of liquid volume fraction, axial droplet velocity and droplet sizes are assumed to be Gaussian:

$$\alpha_l = \alpha_{l,max}.e^{-\frac{r^2}{2\sigma_\alpha^2}} \tag{23}$$

$$U_{axial} = U_{max}.e^{-\frac{r^2}{2\sigma_U^2}} \tag{24}$$

$$d = d_{max}.e^{-\frac{r^2}{2\sigma_d^2}} \tag{25}$$

where $\alpha_{l,max}$, U_{max} and d_{max} are the values on the spray axis on the DITurBC plane, r is the radial coordinate and σ_α^2, σ_U^2, σ_d^2 are the Gaussian width parameters.

Because of the correlation between the distribution of axial velocity and droplet size, the same Gaussian width are assumed for these two profiles: $\sigma_d^2 = \sigma_U^2$. Furthermore, due to the high density of liquid near the nozzle, measurements of droplet sizes are not reliable and there exists no experimental correlation for d_{max}. According to Smallwood et al. [18], the droplet size for Diesel injection is between $5\mu m$ and $15\mu m$. Taking into account that the spray is initialised close to the nozzle exit and that larger diameter may still be present, an arbitrary maximum droplet size of $20\mu m$ is supposed.

The unknown parameters U_{max}, σ_U^2, $\alpha_{l,max}$, σ_α^2 are determined later in Section 4.3 .

The radial distribution of radial velocity is taken from Eq. (19) and assuming linear increase with the radial coordinate. Indeed, the larger droplets remain on the spray axis due to their higher inertia while smaller droplets are more easily entrained by the gas towards the periphery of the spray and therefore gain radial velocity. The formulation is then:

$$U_{rad} = U_{axial} \tan(\phi/2) r/W = U_{max}.e^{-\frac{r^2}{2\sigma_U^2}} \tan(\phi/2) r/W \tag{26}$$

where W is the half width of the spray.

4.3 Determination of Gaussian parameters

The radial distribution of velocity, liquid volume fraction and droplet diameters presented above require to determine the four unknown parameters $\alpha_{l,max}$, U_{max}, σ_α and σ_U.

4.3.1 Gaussian width of the liquid volume fraction profile on the DITurBC plane

The Gaussian width σ_α represents the spray angle and can be expressed as Full Width at Half Maximum (FWHM) which corresponds to the width of half the spray angle $2r_{HM}$. This formulation is traditionally used in experiments [30]. This gives from Eq. (23):

$$\frac{\alpha_{l,max}}{2} = \alpha_{l,max}.e^{-\frac{r_{HM}^2}{2\sigma_\alpha^2}} \tag{27}$$

with $r_{HM} = \tan(\phi/4).Dist + D_{exit}/2$, where $Dist = 10D_{exit}$ is the distance to

the nozzle exit. The Gaussian width is then:

$$\sigma_\alpha = \frac{r_{HM}}{\sqrt{2\ln 2}} = \frac{\tan(\phi/4).Dist + D_{exit}/2}{\sqrt{2\ln(2)}} \tag{28}$$

4.3.2 Velocity on the DITurBC plane

In order to calculate the maximum axial velocity on the DITurBC plane, the empirical formula of Chaves et al. [29] is used:

$$U_{l,max} = U_{Dist} = U_{exit}\left(\exp\left(-\frac{1}{3}\frac{x}{D_{exit}}\frac{\rho_g}{\rho_l}\right)\right)^{0.72} \tag{29}$$

with $x/D_{exit} = 10$.

Concerning the gas axial velocity, two choices may be considered:

- No gas entrainment: the axial gas velocity is zero on the DITurBC plane. This hypothesis may prove interesting because it avoids a gas inflow boundary condition. As demonstrated below, this case is not physically acceptable but its analysis allows a better understanding of the influence of some physical phenomena on the radial distributions.
- Gas entrainment: the idea is to calculate the axial gas velocity by considering the conservation of liquid axial momentum.

These two possibilities are addressed below.

By conservation of the mass flow rate Q between the nozzle exit and the DITurBC plane and given the spray half-width $W = \tan(\phi/2).Dist + D_{exit}/2$, we get:

$$Q = U_{exit}.A_{eff}.\rho_l = \int_0^{2\Pi}\int_0^{W} r\alpha(r)U(r)\rho_l dr d\beta \tag{30}$$

Because of the conservation of axial liquid velocity and in the case of no entrainment (no drag force) one gets $U_{max} = U_{exit}$:

$$Q = 2\Pi\rho_l \int_0^{W} r\alpha(r)U(r)dr = 2\Pi\rho_l \int_0^{W} r\alpha_{l,max}U_{exit} \exp^{-\frac{r^2}{2\sigma_\alpha^2}} \exp^{-\frac{r^2}{2\sigma_U^2}} dr \tag{31}$$

Simplifying with the parameters $\sigma_1^2 = \frac{2\sigma_\alpha^2\sigma_U^2}{\sigma_\alpha^2+\sigma_U^2}$ and integrating by parts gives:

$$Q = \rho_l\alpha_{l,max}U_{exit}\Pi\sigma_1^2\left(1 - \exp^{-\frac{W^2}{\sigma_1^2}}\right) \tag{32}$$

Thus:

$$\alpha_{l,max} = \frac{A_{eff}}{\Pi\sigma_1^2\left(1 - \exp^{-\frac{W^2}{\sigma_1^2}}\right)} \tag{33}$$

If the gas velocity is zero, the liquid axial momentum is conserved:

$$U_{exit}^2.A_{eff}.\rho_l = \int_0^{2\Pi}\int_0^{W} r\alpha(r)U^2(r)\rho_l dr d\beta \tag{34}$$

Integrating by parts gives:

$$U_{exit}^2.A_{eff}. = \Pi U_{exit}^2\alpha_{l,max}\sigma_2^2\left(1 - \exp^{-\frac{W^2}{\sigma_2^2}}\right) \tag{35}$$

with $\sigma_2^2 = \frac{2\sigma_\alpha^2\sigma_U^2}{2\sigma_\alpha^2+\sigma_U^2}$

Using Eq. (33) gives:

$$\sigma_2^2 \left(1 - \exp^{-\frac{W^2}{\sigma_2^2}}\right) = \sigma_1^2 \left(1 - \exp^{-\frac{W^2}{\sigma_1^2}}\right) \tag{36}$$

This equality is verified only if $1/\sigma_U^2 = 0$, that means that the hypothesis of a Gaussian profile on the velocity is wrong. This is in contradiction with what is found experimentally [29]. In conclusion, the Gaussian shape of the liquid axial velocity, observed experimentally, is due to the exchange of axial momentum via drag force between the liquid and the gas.

Furthermore, the mass and axial momentum conservation do not constrain the parameter σ_α^2. The Gaussian shape of the liquid volume fraction is due solely to the spray opening by atomisation. For practical purposes, the hypothesis of a zero axial gas velocity is not compatible with the hypothesis of a Gaussian distribution of axial liquid velocity.

For these reasons, the case of no entrainment is discarded and for the remainder of the paper, the gas velocity has a Gaussian shape supposed similar to that of the liquid radial distribution:

$$U_g = U_{g,max}.e^{-\frac{r^2}{2\sigma_U^2}} \tag{37}$$

As discussed previously, the gas velocity is the result of drag and so depends on the liquid velocity. Therefore, this hypothesis seems to be valid. This implies that the gas phase and the liquid phase are rapidly in equilibrium.

Taking into account the decrease of axial liquid velocity by exchange with the gas phase ($U_{max} < U_{exit}$) and using the mass conservation equation, one obtains:

$$\alpha_{l,max} = \frac{U_{exit} A_{eff}}{U_{l,max} \Pi \sigma_1^2 \left(1 - \exp^{-\frac{W^2}{\sigma_1^2}}\right)} \tag{38}$$

The conservation of axial momentum of the system 'gas+liquid' between the nozzle exit and the DITurBC plane yields:

$$U_{exit}^2 . A_{eff} . \rho_l = \int_0^{2\Pi} \int_0^W r \alpha_l(r) U_l^2(r) \rho_l dr d\beta + \int_0^{2\Pi} \int_0^W r \alpha_g(r) U_g^2(r) \rho_g dr d\beta \tag{39}$$

Using the equality $\alpha_g(r) = 1 - \alpha_l(r)$, one obtains after integration:

$$\begin{aligned} U_{exit}^2 . A_{eff} . \rho_l = & \\ & \Pi U_{l,max}^2 \alpha_{l,max} \rho_l \sigma_2^2 \left(1 - \exp^{-\frac{W^2}{\sigma_2^2}}\right) \\ & + \Pi U_{g,max}^2 \rho_g \sigma_U^2 \left(1 - \exp^{-\frac{W^2}{\sigma_U^2}}\right) \\ & - \Pi U_{g,max}^2 \alpha_{l,max} \rho_g \sigma_2^2 \left(1 - \exp^{-\frac{W^2}{\sigma_2^2}}\right) \end{aligned} \tag{40}$$

with $\sigma_2^2 = \frac{2\sigma_\alpha^2 \sigma_U^2}{2\sigma_\alpha^2 + \sigma_U^2}$

Using Eq. (38) one gets:

$$\begin{aligned} U_{exit}^2 . A_{eff} . \rho_l = & U_{l,max} \frac{U_{exit} A_{eff}}{\sigma_1^2 \left(1 - \exp^{-\frac{W^2}{\sigma_1^2}}\right)} \rho_l \sigma_2^2 \left(1 - \exp^{-\frac{W^2}{\sigma_2^2}}\right) \\ & + \Pi U_{g,max}^2 \rho_g \sigma_U^2 \left(1 - \exp^{-\frac{W^2}{\sigma_U^2}}\right) \\ & - U_{g,max}^2 \frac{U_{exit} A_{eff}}{U_{l,max} \sigma_1^2 \left(1 - \exp^{-\frac{W^2}{\sigma_1^2}}\right)} \rho_g \sigma_2^2 \left(1 - \exp^{-\frac{W^2}{\sigma_2^2}}\right) \end{aligned} \tag{41}$$

σ_α^2 can be expressed in terms of σ_U^2 by using the parameter K defined by $\sigma_\alpha^2 = K \sigma_U^2$. Thus, $\sigma_2^2 = \frac{2}{2K+1} \sigma_\alpha^2$ and $\sigma_1^2 = \frac{2}{K+1} \sigma_\alpha^2$.

$$
\begin{aligned}
U_{exit} = & U_{l,max} \frac{(K+1)}{(2K+1)} \frac{\left(1 - \exp^{-\frac{(2K+1)W^2}{2\sigma_\alpha^2}}\right)}{\left(1 - \exp^{-\frac{(K+1)W^2}{2\sigma_\alpha^2}}\right)} \\
& + \frac{\Pi . U_{g,max}^2 . \sigma_\alpha^2 . \rho_g}{K U_{exit} . A_{eff} . \rho_l} \left(1 - \exp^{-\frac{KW^2}{\sigma_\alpha^2}}\right) \\
& - \frac{(K+1)}{(2K+1)} \frac{U_{g,max}^2 \rho_g}{U_{l,max} \rho_l} \frac{\left(1 - \exp^{-\frac{(2K+1)W^2}{2\sigma_\alpha^2}}\right)}{\left(1 - \exp^{-\frac{(K+1)W^2}{2\sigma_\alpha^2}}\right)}
\end{aligned} \tag{42}
$$

The remaining unknown parameters are K and $U_{g,max}$.

In order to determine $U_{g,max}$, it is assumed that the liquid-gas equilibrium is rapidly achieved. In this case $U_{g,max} = U_{l,max}$. Let us consider the characteristic time Δt, which is the time for the gas to accelerate from zero to the liquid velocity. This time is determined using the axial momentum equation of the gas phase, considering only the drag force:

$$
\alpha_g \rho_g \frac{U_{g,max}}{\Delta t} \approx \alpha_l \rho_l \frac{U_{l,max}}{\tau_p} \tag{43}
$$

The time for the gas to accelerate from zero to the liquid velocity is then:

$$
\Delta t = \frac{\alpha_g \rho_g}{\alpha_l \rho_l} \tau_p \tag{44}
$$

with τ_p the relaxation time defined for a droplet of diameter d defined as:

$$
\tau_p \approx \frac{d^2 \rho_l}{18 \mu_g} \tag{45}
$$

For the worst case, with droplets of diameter $d = 20 \mu m$, one obtains:

$$
\Delta t = 1.310^{-4} s
$$

with $\mu_g = 2.10^{-5} Pa/s$, $\rho_g = 30 kg/m^3$, $\alpha_g = 0.8$, $\alpha_l = 0.2$ and $\rho_l = 800 kg/m^3$. These numerical values correspond to the experiment of Chaves et al. [29] described in section 5.3.

This time is shorter that the needle opening time ($\approx 0.2ms$). Consequently, it is assumed that the gas velocity reaches the liquid velocity before the needle has completely opened. In addition, during this period, the flow is fully unsteady with a spray angle varying in time and the model presented here does not aim to be predictive. The hypothesis $U_{g,max} = U_{l,max}$ is then valid. Furthermore, a turbulent field will be imposed on the boundary condition so that the precision on $U_{g,max}$ is not crucial. The important idea is to ensure the conservation of the mass and momentum fluxes.

Finally, in order to find K it is assumed that:

$$\frac{\left(1 - \exp^{-\frac{(K+2)W^2}{2K\sigma_\alpha^2}}\right)}{\left(1 - \exp^{-\frac{(K+1)W^2}{2K\sigma_\alpha^2}}\right)} \approx 1 \tag{46}$$

In the same way it is presumed that :

$$\left(1 - \exp^{-\frac{W^2}{K\sigma_\alpha^2}}\right) \approx 1 \tag{47}$$

This is the same as integrating mass and axial momentum fluxes between 0 and ∞ instead of 0 and W. Eq. (42) then becomes a second order equation in K:

$$a_2 K^2 + a_1 K + a_0 = 0 \tag{48}$$

with:

$$a_2 = 2U_{exit} - U_{l,max} + \frac{U_{l,max}\rho_g}{\rho_l} \tag{49}$$

$$a_1 = U_{exit} - U_{l,max} - \frac{2\Pi.U_{g,max}^2.\rho_g.\sigma_\alpha^2}{U_{exit}.A_{eff}.\rho_l} + \frac{U_{l,max}\rho_g}{\rho_l} \tag{50}$$

$$a_0 = -\frac{\Pi.U_{g,max}^2.\sigma_\alpha^2.\rho_g}{U_{exit}.A_{eff}.\rho_l} \tag{51}$$

The two solutions of Eq. (48) are: $K_1 = \frac{-a_1+\sqrt{{a_1}^2-4a_2a_0}}{2a_2}$ and $K_2 = \frac{-a_1-\sqrt{{a_1}^2-4a_2a_0}}{2a_2}$. Because $a_2 > 0$ and $a_0 < 0$, the only positive solution is K_1. The negative solution K_2 is discarded because it leads to a non Gaussian shape on the velocity distribution. Finally, knowing K_1 and σ_α^2 and using the expression $\sigma_\alpha^2 = K\sigma_U^2$, one obtains σ_U^2 and then $\alpha_{l,max}$ with Eq. (38).

To resume, the four Gaussian parameters are obtained using Eq. (27) for σ_α^2, Eq. (29) for $U_{l,max}$, Eq. (48) for σ_U^2 and Eq. (38) for $\alpha_{l,max}$.

4.4 Turbulent boundary conditions

The profiles we have obtained for the boundary conditions are mean profiles. A drawback of the boundary conditions is that the history of the gas and liquid flows between the injector exit and the DITurBC plane is lost. For this purpose, we use unsteady boundary conditions that allow us to reproduce the unsteadiness of the flow due to the flow inside the nozzle and the turbulence generated between the nozzle exit and the DITurBC plane. It is assumed that the flow on the DITurBC plane is a consequence of these two phenomena.

In order to create a turbulence field with a given statistical profile, a non-dimensional homogeneous fluctuating velocity field is generated. This field is then rescaled and added to the mean velocity profile on the DITurBC for both liquid and gas phases. The method is based on the work of Kraichnan [31] and

a similar method is used by Smirnov et al.[32].

The use of these turbulent boundary conditions as well as their influence on the spray formation will be described in a future paper.

5 Validation

The model for the DITurBC is validated in two steps. First, by checking the nozzle exit velocity and spray angle, the injector model presented in Section 3 is validated. Then by comparing the modelled radial distributions profiles of velocities with experimental results the construction of the Gaussian profiles in Section 4 are assessed.

5.1 Injection velocity

The validation of the turbulence-cavitation model is achieved by comparison with the experimental measurements of Leick et al. [33] obtained for two different pressures in the chamber (see Table 1). The velocity measurements are made at $1.9mm$ from the nozzle exit at an injection pressure of 22 MPa with a nozzle diameter of $154\mu m$.

As shown in Table 1, the predicted exit velocities are very close to the experimental measurements. The relative difference is 3.6% which is of the same order as the experimental precision, 3% according to Leick et al. [33].

The sub-models for the spray angle are validated by comparison with the experimental data of Blessing et al. [14], who measured spray angles for three nozzles denoted 1,2 and 3 in Table 2. The nozzles used have different conical shape factors leading to different spray angles due to cavitation. The spray angles are measured at the nozzle exit.

Other spray angle measurements may be found in Saliba et al. [34], at $2mm$ from the nozzle exit and for different backpressures. Results are depicted on Fig. 4.

Here again, the accuracy of the model predictions is good, especially for the cases of Blessing et al. [14]. Model results are less accurate for the cases of Saliba et al. [34] but the increase of the angle with the backpressure, an effect described by the aerodynamical spray angle (see Section 4.1), is reproduced. The maximum difference is about 1 degree which is of the same order of magnitude as the variation of the spray angle during injection.

5.3 Axial velocity profile at $10D_{exit}$ from nozzle exit

Chaves et al. [29] have measured the radial distribution of the spray axial velocity at $x/D_{exit} = 10$ from the nozzle exit (see Table 3). This corresponds to a Diesel like liquid injection without cavitation at a moderate pressure ($\Delta P = 10MPa$) into a quiescent dense air ($3MPa$). The injector nozzle diameter is $D = 200\mu m$. The measurements are made after the injection reaches a quasi-steady state. The Bernoulli velocity is $154.7m/s$ for this case.

A first interesting observation is that the absence of cavitation is in agreement with the prediction of the injector model (Eq. (5)). The second interesting observation (see Table 3) is that the discharge coefficient measured by [29] is also well predicted by Eq. (4).

From the shadowgraphy provided by [29], the spray angle is measured and compared to the value obtained with the model. Again, the agreement is very good (see Table 3).

Furthermore, Eq. (47) is a good hypothesis as, for this case, the parameter provided by the model are : $\sigma^2 = 7.710^{-8}$, $K = 0.48$, $W = 7.10^{-4}$ and then $\left(1 - \exp^{-\frac{W^2}{K\sigma_\alpha^2}}\right) \approx 0.999$. The parameter $K = 0.48$ means that the Gaussian on the liquid volume fraction is about two times larger than the Gaussian on the axial liquid velocity. Therefore, high velocites droplets are concentrated near the spray axis. In addition, the model gives $\alpha_{l,max} = 0.2$ what confirms that the spray is fully dispersed (no liquid core) at ten nozzle diameters from the nozzle exit.

Finally, the radial distributions of mean axial spray velocity are reported in Fig 5 and confirms the good predictivity of the model for the mean profiles.

6 Concluding remarks

In this paper, a model for liquid injection boundary conditions, called DI-TurBC, has been presented. The model uses characteristic features of the injection to build an algebraic description of all spray characteristics and profiles near the nozzle exit.

These profiles can be used as boundary conditions for the Eulerian-Eulerian simulation of Diesel Sprays especially in Large Eddy Simulation. By initialising the spray slightly downstream from the nozzle exit, the DITurBC model allows 3D simulation without solving the complex spray physics at the nozzle exit. Furthermore, this methodology avoids to mesh the nozzle exit, a zone requiring very small mesh size, resulting in a decrease of the computational cost.

The boundary conditions are based on an injector model that determines whether the flow inside the nozzle is cavitating. Knowing the flow regime and the intensity of turbulence and cavitation, the velocity and the spray angle at the nozzle exit are deduced. Then, by the application of conservation laws, velocity, liquid volume fraction, and droplet size profiles are calculated at a given distance downstream from the nozzle exit, which represent the boundary condition DITurBC. These mean profiles are assumed to be Gaussian. The Gaussian widths of velocity and liquid volume fraction are found to be different and the conservation laws of mass and axial momentum permit us to exhibit a relation between them.

The model has been validated against numerous experiments guarantying reliable boundary conditions.

The implementation of DITurBC in the AVBP CFD code [35] has been done. LES of Diesel Sprays using these DITurBC is under preparation and will be published in a future paper.

References

[1] Ryan T.W., Callahan T.J.. Homogeneous CHarge Compression Ignition (HCCI) of Diesel Fuel. *SAE 961160.* 1996.

[2] Lu X-C., Chen W., Huang Z.. A fundamental study on the control of the HCCI combustion and emissions by fuel design concept combined with controllable EGR. Part 1. The basic characteristic of HCCI combustion. *Fuel.* 2005;84:1074-1083.

[3] Ozdor N., Dulger M., Sher E.. Cyclic variability in spark ignition engines. A literature survey *SAE.* 1994;950683.

[4] Launder B.E., Spalding D. B.. *Mathematical models of turbulence.* Academic Press 1972.

[5] Drake M.C., Haworth D.. Advanced gasoline engine development using optical diagnostic and numerical modeling *Proceedings of the* 31^{st} *Symposium (Int.) on Combustion, The Combustion Institute.* 2007.

[6] Sagaut P.. *Large Eddy Simulation for incompressible flows.* Scientific computation seriesSpringer-Verlag 2000.

[7] Selle L., Benoit L., Poinsot T., Nicoud F., Krebs W.. Joint use of Compressible Large-Eddy Simulation and Helmoltz solvers for the analysis of rotating modes in an industrial swirled burner *Combust. Flame.* 2006;145:194-205. NF.

[8] Schmitt P., Poinsot T.J., Schuermans B., Geigle K.. Large-eddy simulation and experimental study of heat transfer, nitric oxide emissions and combustion instability in a swirled turbulent high pressure burner *J. Fluid Mechanics.* 2007;570:17-46.

[9] Richard S., Colin O., Vermorel O., Benkenida A., Angelberger C., Veynante D.. Towards large eddy simulation of combustion in spark ignition

engines *Proc. of the Combustion Institute.* 2007;31. tpimft.

[10] Vermorel O., Richard S., Colin O., Angelberger C., Benkenida A.. Multi-cycle LES simulations of flow and combustion in a PFI SI 4-valve production engine *SAE PAPER 2007-01-0151.* 2007.

[11] Abraham J.. What Is Adequate Resolution in the Numerical Computations of Transient Jets? *Trans. of the SAE.* 1997;106:141-155.

[12] Iyer V., Abraham J.. Penetration and Dispersion of Transient Gas Jets and Sprays *Combustion. Sci. and Tech..* 1997;130:315-335.

[13] Subramaniam S., O'Rourke P.. Numerical Convergence of the KIVA-3 Code for Sprays and Its Implications for Modeling *Los Alamos Lab. Rep. UR-98-5465, Los Alamos, NM.* 1998.

[14] Blessing M., Knig G., Krger C., Michels U., Schwarz V.. Analysis of flow and cavitation phenomena in diesel injection Nozzles and its effets on spray and mixture formation *SAE.* 2003;2003-01-1358.

[15] Hiroyasu H.. Spray break-up mechanism from the hole-type nozzle and its applications *Atomization and Sprays.* 2000;10:511-527.

[16] Sou A., Hosokawa S., Tomiyama A.. Effects of cavitation in a nozzle on a liquid jet atomization *Int. J. Heat and Mass Transfer.* 2007;50:3575-3582.

[17] Habchi C., Dumont N., Simonin O.. Multidimensional Simulation of Cavitating Flows in Diesel Injectors by a Homogeneous Mmixture Modeling Approach *Atomization and Sprays.* 2008;18:129-162.

[18] Smallwood G., Gulder O.. Views on the structure of transient diesel sprays *Atomization and Sprays.* 2000;10:355-386.

[19] Ueki H., Ishida D., Naganuma M.. Simultaneous Measurements of Velocity and size of diesel fuel near nozzle orifice by Laser 2-Focus velocimeter with Micro-Scale probe volume THIESEL 2004 Conference on Thermo-

and fluid Dynamic Processes in Diesel Engines 2004.

[20] Soteriou C., Andrews R., Smith M.. Direct injection Diesel Sprays and the Effect of Cavitation and Hydraulic flip on Atomization *SAE.* 1995;950080.

[21] Yue Y., Powell C.F., Poola R., Wang J., Schaller J.K... Quantitative measurements of diesel fuel spray characteristics in the near-nozzle region using x-ray absorption *Atomization and Sprays.* 2001;11:471-490.

[22] Tanner F. X., Feigl K. A., Ciatti S. A., et al. Structure of high-velocity dense sprays in the near-nozzle region *Atomization and Sprays.* 2006;16:579-597.

[23] Sarre C., Kong S.C., Reitz R.D.. Modeling the Effects of Injector Nozzle Geometry on Diesel Sprays *SAE PAPER 1999-01-0912.* 1999.

[24] Nurick W.H.. Orifice cavitation and its effect on spray mixing *Journal of Fluids Engineering.* 1976;98:681-687.

[25] Benedict R. P.. *Fundamentals of pipe flows.* Wiley, New York 1980.

[26] Nishimura A., Assanis D. N.. A Model for Primary Diesel Fuel Atomization Based on Cavitation Bubble Collapse Energy in *ICLASS2000*(Pasadena, CA) 2000.

[27] Huh K.Y., Gosman A.D.. A phenomenological Model for Diesel Spray Atomization International Conference On Multiphase Flows'91 1991.

[28] O'Rourke P.J., Amsden A. A.. The tab method for numerical calculation of spray droplet breakup *SAE.* 1987;872089.

[29] Chaves H., Kirmse C., Obermeier F.. Velocity measurement of dense diesel fuel sprays in dense air *Atomization and Sprays.* 2004;14:589-609.

[30] Powell C.F., Ciatti S. A., Cheong S.-K., Lu J., Wang J.. X-Ray Absorption Measurements of Diesel Sprays and the Effects of Nozzle Geometry *SAE PAPER 2004-01-2011.* 2004.

[31] Kraichnan R.H.. Diffusion by a Random Velocity Field *Physics of Fluids.* 1970;13:22-31.

[32] Smirnov A., Shi S., Celik I.. Random flow generation technique for large eddy simulations and particle-dynamics modeling *Trans. ASME. Journal of Fluids Engineering.* 2001;123:359–371.

[33] Leick Ph., Bittlinger G., Tropea C.. Velocity Measurements in the near nozzle region of common-rail diesel sprays at elevated back-pressures 19th Annual Meeting of The Institute for Liquid Atomization and Spray Systems (Europe) 2004.

[34] Saliba R., Baz I., Champoussin J-C., Lance M., Mari J-L.. Cavitation effect on the near nozzle spray development in high pressure diesel injection. 19th Annual Meeting of The Institute for Liquid Atomization and Spray Systems (Europe) 2004.

[35] Moureau V., Lartigue G., Sommerer Y., Angelberger C., Colin O., Poinsot T.. Numerical methods for unsteady compressible multi-component reacting flows on fixed and moving grids *Journal of Computational Physics.* 2004;202:710-736. NF.

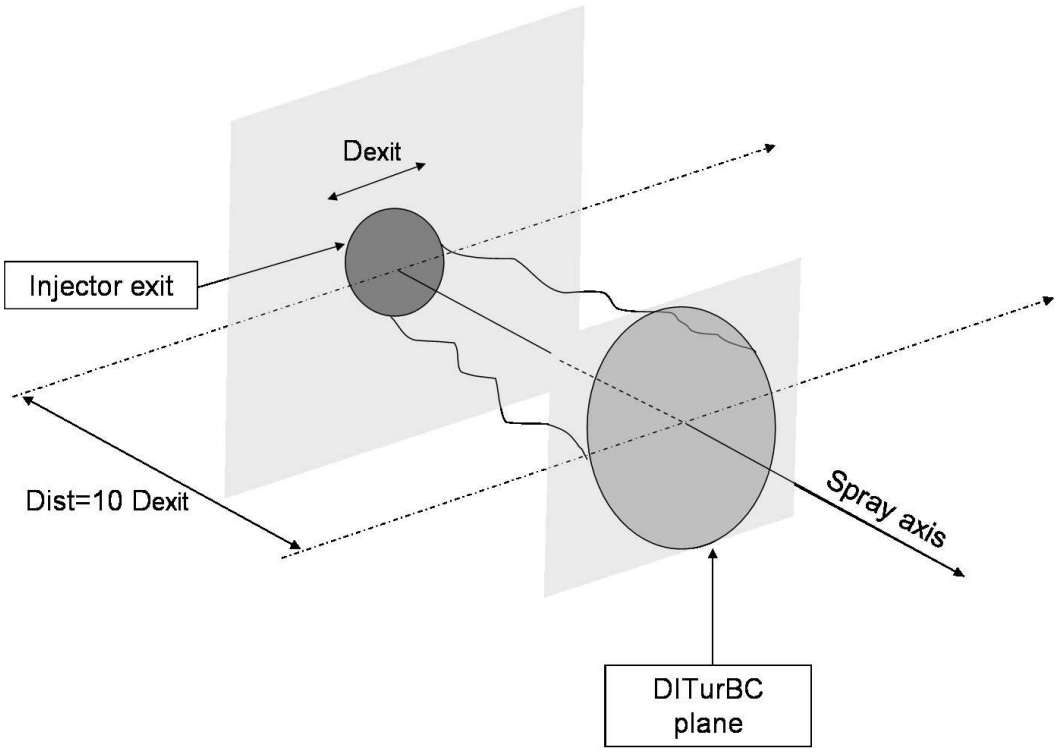

Figure 1. A schematic representation of the location of boundary conditions provided by the DITurBC model.

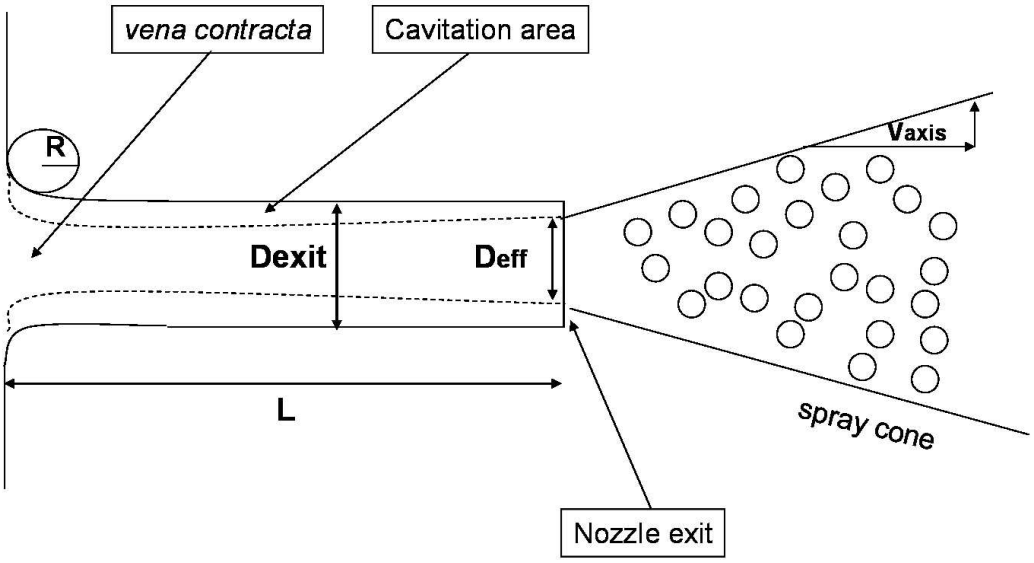

Figure 2. Nomenclature of the injector geometry.

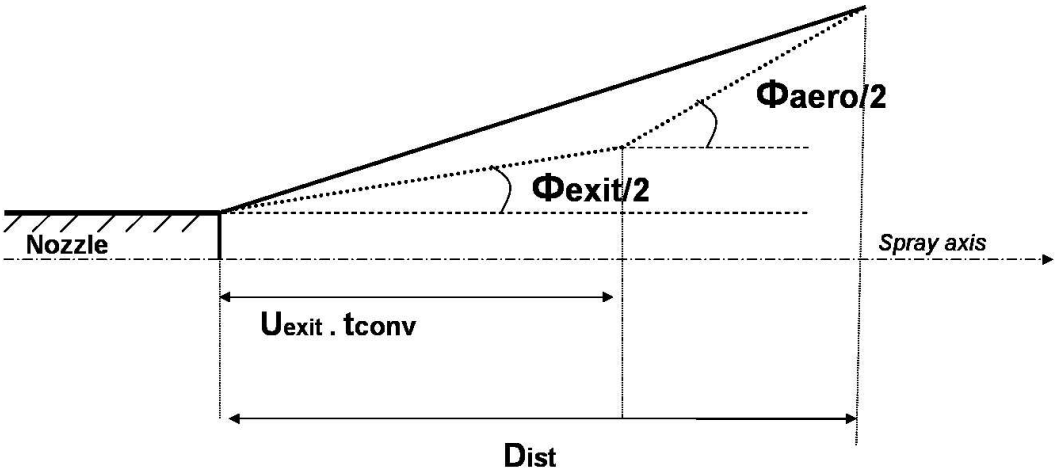

Figure 3. Scheme on the determination of spray angle at distance $Dist$ downstream from the nozzle exit.

Case	I	II
Injection pressure P_{inj} (MPa)	22	22
Chamber pressure P_{ch} (MPa)	0.1	2
Spray exit velocity (m/s): experiment	210-220	185-205
Spray exit velocity (m/s): model	228	187

Table 1

Comparison of spray exit velocity with experimental data of [33]

Number of the nozzle	Spray angle (degrees) Experiment	Spray angle (degrees) DITurBC
1	5.5	6
2	10	9.6
3	13	13.5

Table 2

Comparison of the spray angle predicted by the model with the experiment of [14] for three different nozzles.

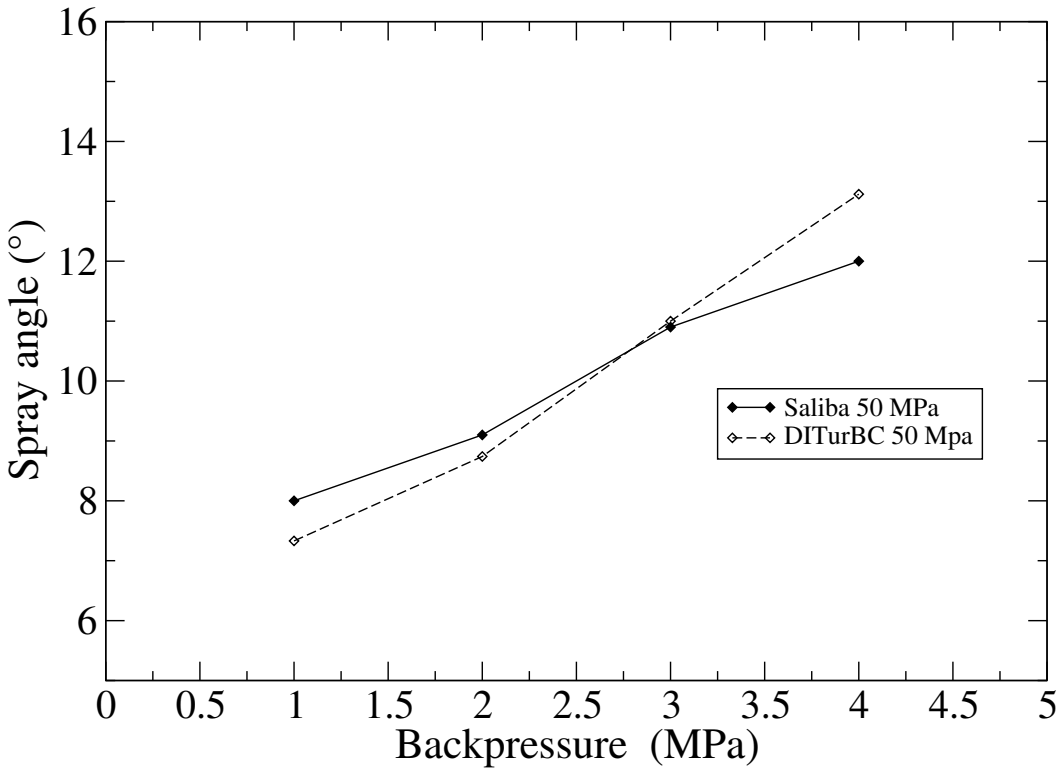

Figure 4. Comparison of the spray angle predicted by the model with the experiments of [34] at $x = 2mm$ for different injection pressures.

P_{inj}	130
P_{ch}	30
Discharge coefficient *via* experiment	0.88
Discharge coefficient *via* model	0.88
Spray angle *via* experiment (degrees)	8.5
Spray angle *via* model (degrees)	7.7

Table 3

Comparison of discharge coefficient and spray angle provided by the model with experimental data of [29]

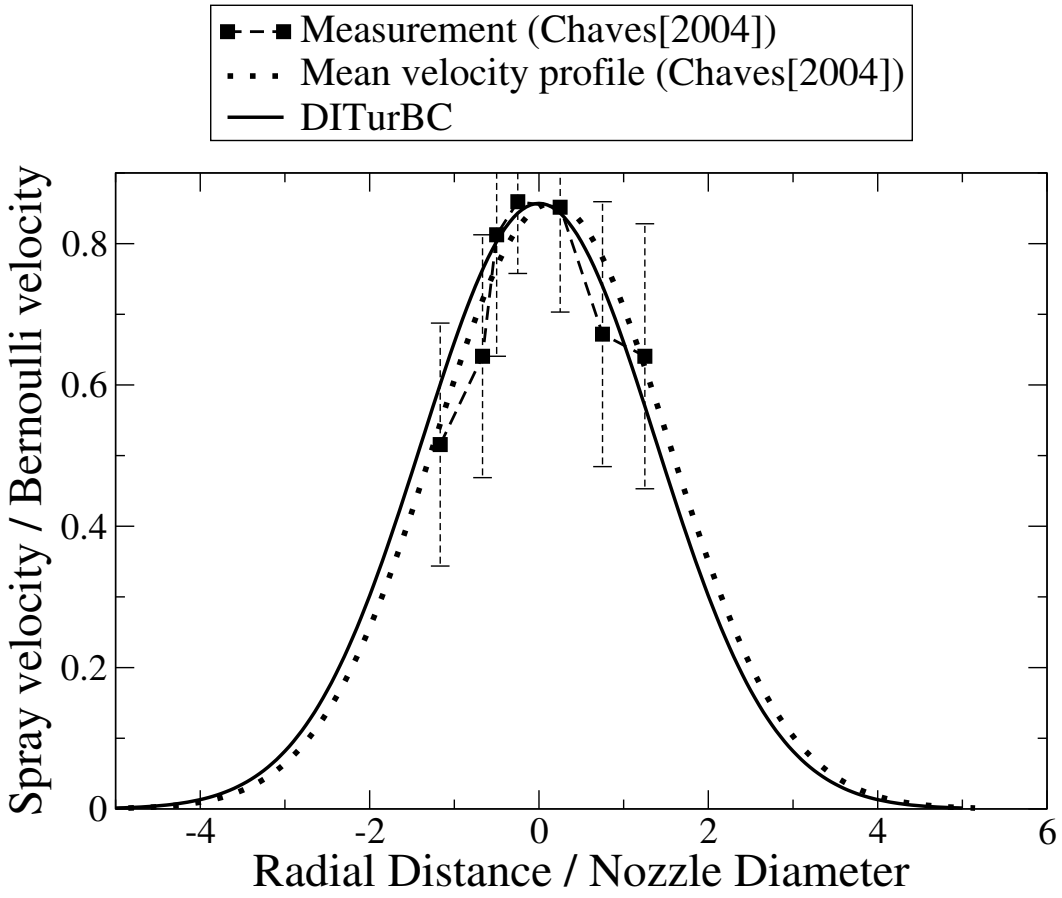

Figure 5. Comparison of radial distribution of spray axial velocity with experimental data of [29] at $x/D_{exit} = 10$